# Exploring the Maze of Cycloserine Conformers in the Gas Phase Guided by Microwave Spectroscopy and Quantum Chemistry

Elena R. Alonso,[†] Marco Fusè,[‡] Iker León,[¶] Cristina Puzzarini,[§] José L. Alonso,[*,¶] and Vincenzo Barone[*,‡]

[†]*Instituto Biofisika (UPV/EHU, CSIC), University of the Basque Country, Leioa,Spain. Fundación Biofísica Bizkaia / Biofisika Bizkaia Fundazioa (FBB), Barrio Sarriena s/n, Leioa, Spain*

[‡]*SMART Laboratory, Scuola Normale Superiore di Pisa, piazza dei Cavalieri 7, 56126 Pisa, Italy*

[¶]*Grupo de Espectroscopia Molecular (GEM), Edificio Quifima, Laboratorios de Espectroscopia y Bioespectroscopia Parque Cientifico UVa, Universidad de Valladolid, 47005 Valladolid (Spain).*

[§]*Dipartimento di "Chimica Giacomo Ciamician", University of Bologna, via F. Selmi 2, 40126, Bologna, Italy*

E-mail: jlalonso@qf.uva.es; vicenzo.barone@sns.it

**Abstract**

Cycloserine shares the five-membered ring with isoxazolidines, which are important scaffolds for drug-design exhibiting diverse biological activities. The most remarkable feature of these compounds is the presence of the N-O bond framed in a cyclic moiety. The lack of an accurate characterization of this structural feature in an isolated system calls for a state-of-the-art theoretical-experimental study.

A quantum-chemical investigation of cycloserine unveiled the presence of eleven local energy minima, with only two of them being separated by significant barriers. This picture has been experimentally confirmed: two species have been unequivocally detected in the gas phase by means of laser ablation microwave spectroscopy, also disentangling the complicated hyperfine structure originating from the presence of two nitrogen atoms.

A thorough characterization of cycloserine and isoxazolidine, benchmarked by the semi-experimental investigation of hydroxilamine, provided the first accurate determination of their structures and pointed out that the rev-DSD-PBEP86 functional is competitive with respect to explicitly-correlated coupled-cluster computations. This outcome paves the way toward accurate studies of large flexible molecules.

# Introduction

Cycloserine (4-amino-3-isoxazolidinone) is a broad-spectrum antibiotic sold under the brand name seromycin, which is still widely used for the treatment of tuberculosis.[1] In 1955, it was extracted from a species of streptomyces[2] and nearly simultaneously prepared synthetically.[3] More recently, its use has been extended to the clinical treatment of anxiety and obsessive–compulsive disorders owing to its action on N-methyl-D-aspartate (NMDA) receptors.[4–7]

In neutral aqueous solution, cycloserine exists in the zwitterionic form, whereas the protonated structure predominates at acidic pH. Under mildly acidic conditions, however, it

hydrolyzes to serine and hydroxylamine.[8] In organic solvents, instead, the ketonic form is the most favored.[2,9] The unsolvated state has attracted some interest because of the agonist activity in the NMDA receptor.[10] Indeed, the interaction between cycloserine and the receptor cavity can be described in terms of the naked species/fragments because of the extensive desolvation the drug undergoes.

While in ref. 10 the study focused on the analysis of HOMO-LUMO energies (which are considered important to discriminate the agonist and antagonist activity), the structure and properties of cycloserine in the gas phase have been recently investigated using infrared multiphoton dissociation (IRMPD), Ultraviolet and X-ray photoelectron (UPS and XPS) spectroscopies, complemented by semi-quantitative quantum-chemical (QC) computations. However, these studies were not able to unambiguously determine the number and structure of low-lying conformers.[11–13]

Cycloserine shares the saturated five-membered ring with isoxazolidines (see Figure 1**b**), a class of compounds that are part of several natural products and have attracted considerable interest in the past decade.[14] Indeed, isoxazolidines are important scaffolds in drug-design chemistry and exhibit interesting diverse biological activities (see, ref. 14 and references therein). The most remarkable feature of this five-membered ring is the presence of adjacent nitrogen and oxygen atoms, which is rarely found in natural products, but represents an important synthetic intermediate, possibly because of the labile nature of the N-O bond. To the best of our knowledge, an accurate characterization of this type of bond framed in a cyclic moiety is entirely missing even though being important for different areas of chemistry.

Since, as mentioned above, the isolated (unsolvated) molecule is of particular interest, a gas-phase study can deliver the lacking information. Rotational spectroscopy is the technique of choice for accurate structural characterizations,[15,16] also being able to unequivocally identify all low-energy isomers, tautomers and/or conformers separated by barriers sufficiently high to avoid interconversion[17,18] and to determine their structural fingerprints.[19–22] In guiding experiments and interpreting the acquired spectra, powerful support is offered by

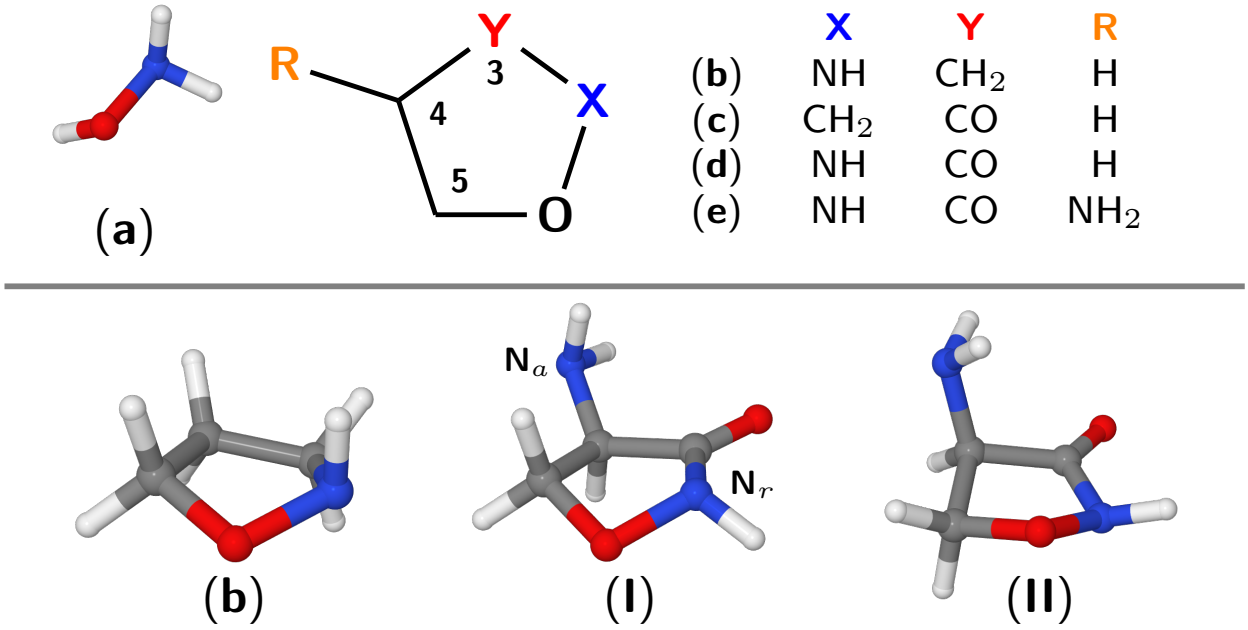


Figure 1: Top panel (investigated molecular systems): (**a**) hydroxylamine; (**b**) isoxazolidine; (**c**) dehydro-3(2H)-furanone; (**d**) 3-isoxazolidinone; (**e**) cycloserine. Bottom panel: the most stable structure of isoxazolidine (**b**) and the two identified structures (**I** and **II**) of cycloserine.

state-of-the-art QC calculations.[15,19,23–26] The synergism of theory and experiment is particularly important whenever flexible molecules, often showing a flat potential energy surface (PES), are investigated.[19,24–29] Furthermore, such a synergism is mandatory for any accurate structural determination.

The rotational spectroscopy techniques used in the characterization of biomolecule building blocks usually exploit laser ablation for their vaporization and an adiabatic expansion of the vaporized sample together with a noble gas carrier. During the expansion metastable isomers are subject to relaxation through collisions when the interconversion barrier is lower than a threshold, which –for a variety of systems– has been found close to 400 $cm^{-1}$ (≈5 kJ $mol^{-1}$) with the expansion starting at room temperature.[30–32] Therefore, an exhaustive search of the low-energy minima combined with the accurate evaluation of their relative stability and the characterization of interconversion barriers is needed whenever previous results are not available. In the case of cycloserine, the two quadrupolar nitrogen nuclei originate a complicated hyperfine structure in the rotational spectrum,[33,34] which becomes

even more severe due to the flexibility of the system that leads to the concomitant presence of different minima of comparable stability. Therefore, the investigation of isolated cycloserine represents a challenging task, from both an experimental and computational point of view.

# Methodology

## Computational Details

Based on our previous experience,[35,36] the structures and harmonic force fields of all the stationary points of cycloserine were obtained employing the double-hybrid rev-DSD-PBEP86 functional[37] in conjunction with the jun-cc-pVTZ triple-zeta basis set,[38,39] also incorporating the D3BJ dispersion correction.[40] This level of theory is hereafter denoted as rDSD. Improved electronic energies for the most significant low-energy minima and the transition states ruling their interconversion were obtained by exploiting explicitly-correlated CCSD(T)-F12[41] computations within the so-called CCSD(T)-F12/CBS+CV composite scheme[42,43] (hereafter CCF12). Briefly, while interested readers can find a detailed description of this model in ref. 42 and in the supporting information (SI), we mention that CC12 recovers basis-set truncation errors and accounts for core-correlation effects. Furthermore, in order to improve the estimated rotational constants (the leading terms in rotational spectroscopy), whose equilibrium values only depend on the equilibrium structure, the geometries of the two stable species envisaged as experimentally detectable (*vide infra*) have been optimized using CCSD(T)-F12 in conjunction with the cc-pVDZ-F12 basis set.[44] This level of theory (hereafter DZF12) leads to results comparable with those delivered by conventional CCSD(T)[45] computations in conjunction with quadruple-zeta basis sets at a much reduced cost.[46] While, as mentioned above, equilibrium rotational constants are straightforwardly obtained from equilibrium geometries, to predict the experimental features, we need to move from the bottom of the well to the vibrational ground state. The same applies also to other spectroscopic parameters, such as the nuclear quadrupole-coupling constants. Vibrational corrections to both types of

constants were computed at the B3LYP-D3BJ/jul-cc-pVDZ level[38,40,47] (hereafter B3) in the framework of second-order vibrational perturbation theory (VPT2).[48] A detailed account of the computational methodology is provided in the SI.

## Experimental Details

The thermal instability of cycloserine due to its high melting point (≈155°C) and the low vapor pressure prevent easy measurements of its gas-phase spectra by standard heating procedures, laser ablation (LA) thus being the only viable option to bring this molecule to the gas phase. The first step of the experimental spectroscopic characterization of cycloserine was carried out using a chirped pulse (CP) Fourier Transform (FT) microwave (MW) spectrometer, based on the pioneering design proposed by the Pate's group,[49] coupled with a laser ablation system (LA-CP-FTMW spectrometer).[50,51] A commercial solid sample of cycloserine was ground and mixed with a minimum amount of a commercial binder and pressed into cylindrical rods, which were placed in an ablation nozzle and vaporized using a Nd:YAG picosecond laser. Then, cycloserine molecules were seeded in the carrier gas Ne at a backing pressure of  10 bar, to expand adiabatically into the vacuum chamber.

In the LA-CP-FTMW spectrometer, an arbitrary waveform generator creates a chirped pulse from 6 to 16 GHz, which is directly amplified by a 300 W traveling wave tube amplifier. The conventional microwave horns have been replaced by the parabolic reflector system composed by dual ridge horns, and two parabolic reflectors (40 cm diameter) separated 70 cm in a paraxial beam configuration. The excitation pulse emerges from a horn antenna to polarize the molecules arising from the laser ablation nozzle located at the center of one of the parabolic reflectors. A second ridge horn antenna is used to detect the free induction decay signal (FID), which is finally amplified and digitized on a fast oscilloscope. This technique makes it possible to record a full range of frequencies spectra in a single acquisition by employing polarization pulses consisting of short and intense microwave chirps in broadband excitation schemes.The molecules present in the supersonic jet are rotationally

cooled to temperatures below 4 K, thus, populating the lower energy levels and increasing the intensity of the transitions originating from them. The broadband rotational spectrum of the laser-ablated cycloserine in the 6-16 GHz frequency range is shown in Figure 2a.

A laser ablation molecular beam (MB) Fourier transform microwave (LA-MB-FTMW) spectrometer[52–55] was used to record the cycloserine spectrum to fully resolve the hyperfine structure due to the presence of two $^{14}$N nuclei (*vide infra*). The optimal conditions to

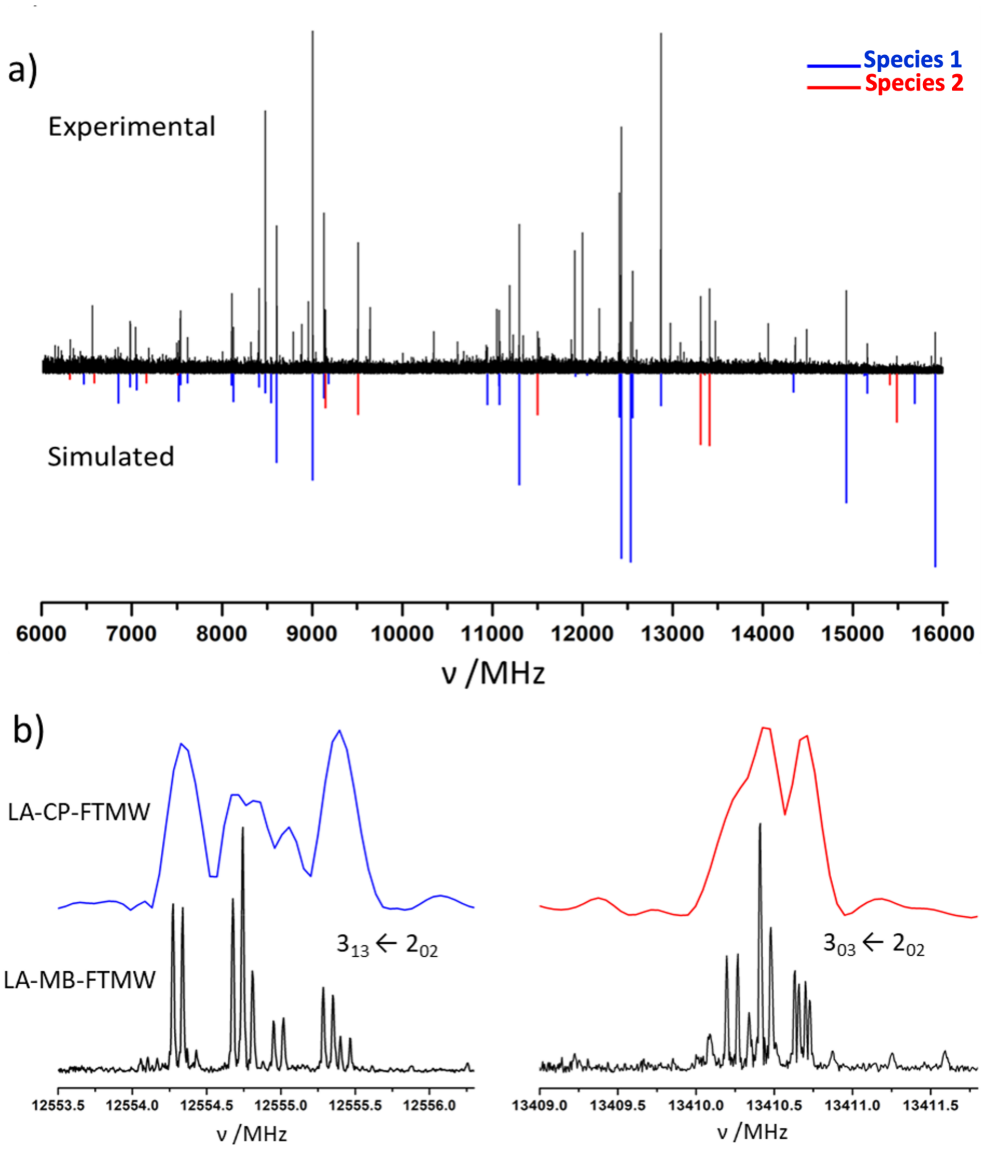


Figure 2: a) Broadband LA-CP-FTMW spectrum of cycloserine recorded in the 6-16 GHz range. b) Resolution comparison between LA-CP-FTMW and LA-MB-FTMW spectra.

polarize the molecules in the jet correspond to molecular pulses of about 1.1 ms, followed by MW polarization pulses of 0.3 $\mu$s duration with powers of 1−40 mW. The microwave FID was recorded for 100 $\mu$s in the time domain at 40−100 ns sample intervals, and Fourier transformed to the frequency domain. Due to the collinear disposition of the supersonic jet and the microwave resonator axis, all emission signals appear split into Doppler doublets (Figure 2b). The arithmetic mean of the doublets was taken as the rest frequency. From 50 to 250 averages were phase-coherently co-added to achieve a reasonable signal-to-noise ratio. The estimated accuracy of the frequency measurements is thus better than 3 kHz.

# Results & Discussion

Cycloserine has three soft degrees of freedom, namely the rotation of the $NH_2$ group, the NH inversion and the ring puckering, with the latter being conveniently described in terms of the so-called ring-puckering or Cremer–Pople coordinates.[56,57] In particular, for five-membered rings, one puckering amplitude **q** and one pseudorotation angle $\theta$ are sufficient to describe the displacement of all the atoms with respect to a mean plane. Since **q** usually changes by 0.2-0.3 Å at most, $\theta$ is the essential degree of freedom to define the ring conformation, with the twisted (T) and bent (B) structure of the cycle corresponding to stationary points. The nomenclature used for defining the different structures employs apices or pedices to indicate the atoms lying above or below the mean plane defined in the Cremer–Pople reference frame (see Figure S1 in SI). Furthermore, the standard Cahn-Ingold-Prelog rules are followed for labeling the stereogenic nitrogen atom as R or S.[58]

To derive the possible energy minima of cycloserine, we can proceed step by step (see Figure 1 and Figures S1 and S2 in the SI). The ring puckering is characterized by only two non-equivalent twisted energy minima ($^5T_O$ and $_5T^O$), which are actually equivalent enantiomers in the absence of the $NH_2$ moiety (i.e., for the model compounds **b**, **c**, and **d** of Figure 1). The presence of the NH group (like in 3-isoxazolidinone, Figure 1 **d**) splits each

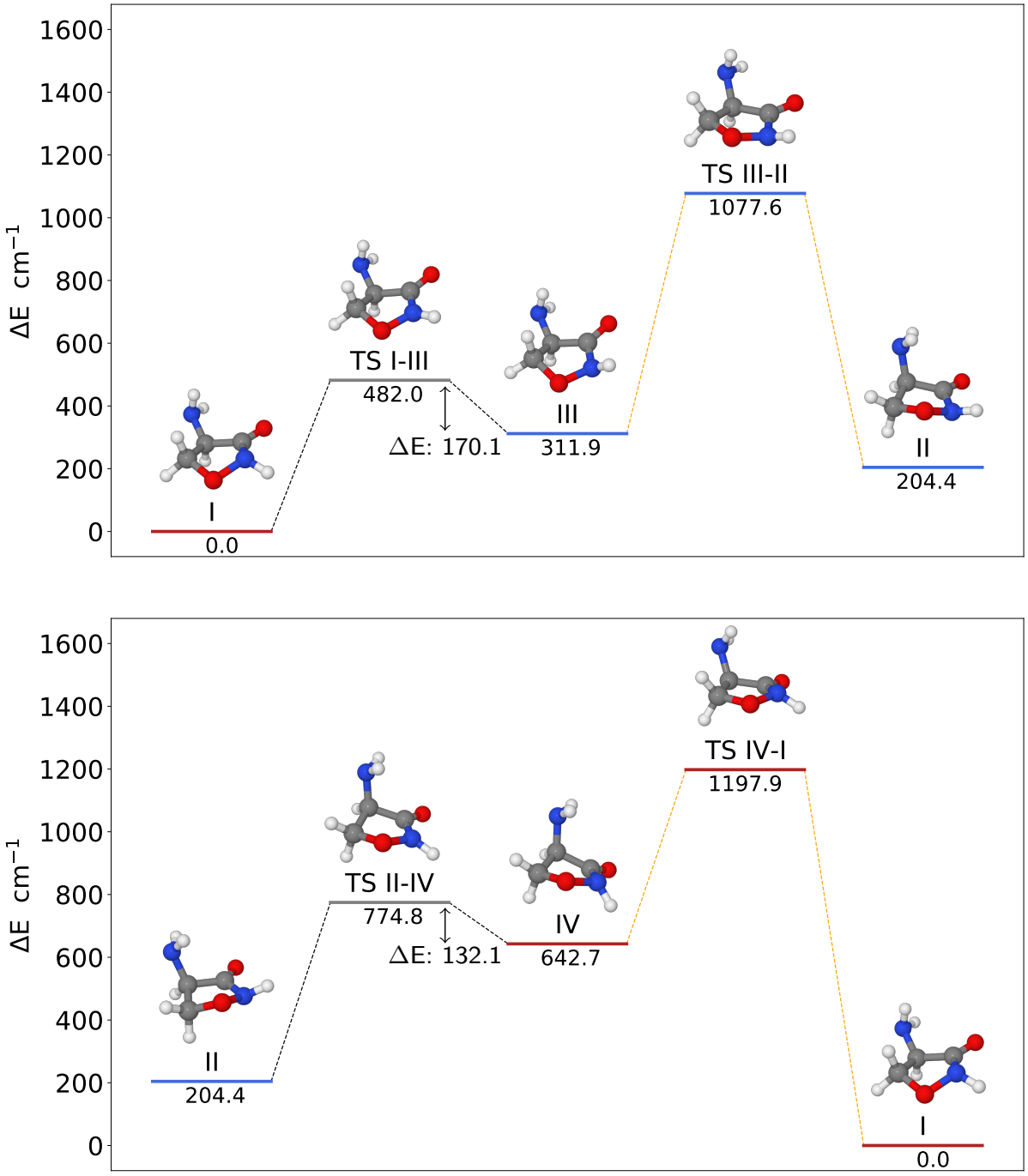


Figure 3: Step-wise mechanism connecting the two most stable species (**I** and **II**) of cycloserine. Red segments denote structures with $S_N$ configuration, while the blue ones those with $R_N$ configuration. The reported relative energies (in cm$^{-1}$) are computed at the CCF12 level.

minimum in two forms due to the NH inversion (described by the $\omega$ angle between the NH bond and the plane containing the NO and $NC_3$ bonds[59]). Finally, the $NH_2$ rotation (described by the $\tau$ dihedral angle: $C_5$-$C_4$-$N_a$-H) is characterized by three staggered conformers, namely two gauche ($G^+$ and $G^-$) and one anti (A) structure. Overall, a total of 12 energy minima is thus expected for cycloserine, but one of them has not been found, at least at the level of theory considered (see Tables S1 and S2 of the SI).

All the energy minima and transition states related to ring puckering and NH inversion share the same profile for the $NH_2$ rotation (see Figures S3 and S4 of the SI), thus allowing to consider this degree of freedom essentially decoupled from the others. Moreover, in all cases, the negligible barrier governing the $NH_2$ rotation suggests the full relaxation to the most stable rotamer $G^-$ (i.e. $\tau \sim 300°$) under the conditions of rotational spectroscopy experiments. Therefore, in the following, the specification of the $\tau$ value is skipped in the enumeration and labeling of the energy minima. The two most stable structures of the cycloserine ring are ${}_5\mathrm{T}^{\mathrm{O}}S_N$ (hereafter **I**) and ${}^5\mathrm{T}_{\mathrm{O}}R_N$ (hereafter **II**), which have opposite configuration of the NH nitrogen atom ($\omega \approx \pm 44°$), a nearly constant amplitude of 0.37-0.38 Å, and pseudo-rotation phases of -13° and 164°, respectively.

In Figure 3, the energy profiles connecting **I** and **II** through the step-wise mechanisms of ring puckering and NH inversion are sketched. The transition states ruling these interconversions are intermediate between those expected for ring inversion and pseudo-rotation. Furthermore, the NH inversion is always governed by quite small energy barriers. Therefore, the less-stable energy minima related to this motion, namely ${}^4\mathrm{T}_5R_N$ (hereafter **III**) and ${}_4\mathrm{T}^5S_N$ (hereafter **IV**), are expected to easily relax to **I** and **II** under the experimental conditions. Indeed, the relaxation of **III** to **I** and of **IV** to **II** are ruled by barriers of only 170 and 132 $cm^{-1}$, respectively (see Tables S1 and S2 of the SI, and Figure 3).

The structures of all the energy minima and transition states discussed above are depicted in Figure 3 and Figure S3 of the SI, whereas the relative energies are given in Tables S1 and S2, with the former table also reporting the spectroscopic parameters of relevance to this

study. At the CCF12 level, **I** has been found 204.4 $cm^{-1}$ more stable than **II**. It is noteworthy that the rDSD model delivers results very close to those issuing from the highly accurate (but also computationally expensive) CCF12 composite scheme. Indeed, the root mean square deviation (RMSD) and maximum absolute error (MAE) of the former with respect to the latter are as low as 20 and 53 $cm^{-1}$, respectively (see Table S1). The widely used B3LYP functional is significantly less accurate, the corresponding RMSD (114 $cm^{-1}$) and MAE (290 $cm^{-1}$) being more than four and five times larger, respectively.

Before proceeding with a thorough analysis of the rotational spectrum, this was cleaned from all known photo-fragmentation lines (e.g., $C_2H_3CN$ and $HC_3N$).[60] Guided by computational simulations of the rotational spectra for the **I** and **II** species (based on the spectroscopic parameters of Table 1), spectral searches in wide frequency regions revealed the presence of two set of characteristic quadruplets that could be assigned to the $\mu_b$-type R-branch $(J+1)_{0,J+1} \leftarrow J_{1,J}$ and $(J+1)_{1,J+1} \leftarrow J_{0,J}$ and $\mu_a$-type R-branch $(J+1)_{1,J+1} \leftarrow J_{1,J}$ and $(J+1)_{0,J+1} \leftarrow J_{0,J}$ transitions, with $J$=2 and $J$=3, of a first species (hereafter Species 1).

As mentioned in the introduction, cycloserine possesses two quadrupolar nuclei, the $^{14}N$ atoms, having nuclear spin I=1. The quadrupole coupling interaction produces splittings of the rotational energy levels, which result into frequency splittings of the rotational transitions (hyperfine structure). The concomitant presence of two quadrupolar nuclei splits each rotational transition into several hyperfine components, thus increasing the line congestion in the spectrum, and –consequently– the difficulty of its interpretation.[33,34] The hyperfine structure is not well resolved by the typical resolution of the broadband LA-CP-FTMW spectrometer (see Figure 2b). Therefore, in the first step, only the frequency centers of each rotational transition were considered. In an iterative process of measuring and fitting, we were able to locate other $\mu_a$ and $\mu_b$ R-branch transitions. All measured transitions were included in a rigid-rotor model analysis to obtain a preliminary set of rotational constants (see Table S4 of the SI), which are in remarkable agreement with those predicted for the global energy minimum, namely the **I** structure.

In the search for another species (hereafter Species 2), a set of weaker transitions with a characteristic common triad pattern was identified and assigned to the $\mu_a$-type R-branch ($J + 1)_{1,J+1} \leftarrow J_{1,J}$, $(J + 1)_{0,J+1} \leftarrow J_{0,J}$, and $(J + 1)_{1,J} \leftarrow J_{1,J-1}$ transitions, with $J$=1 and $J$=2, thus leading to a preliminary set of rotational parameters matching those predicted

**Table 1: Experimental spectroscopic parameters[a] (in MHz, if not otherwise stated) of the Species 1 and 2 of cycloserine are compared with those computed for the I and II structures.**

| | Cycloserine **I** | | | | |
|---|---|---|---|---|---|
| | Equilibrium | | $\Delta$vib[b] | Exp. (Species 1) | |
| | rDSD | DZF12[c] | B3 | $B_0$ | $B_e^{semi}$ |
| A | 3677.68 | 3686.33 | -19.38 | 3684.9725(13) | 3704.34 |
| B | 3173.31 | 3177.13 | -29.20 | 3160.4656(18) | 3189.65 |
| C | 1819.80 | 1824.64 | -16.50 | 1815.46095(33) | 1831.97 |
| $\chi_{aa}N_r$ [d] | 1.7344 | 1.7112 | -0.0247 | 1.7055(47) | |
| $\chi_{bb}N_r$ | 3.6101 | 3.5631 | -0.0136 | 3.6032(38) | |
| $\chi_{cc}N_r$ | -5.3445 | -5.2743 | 0.0383 | -5.3088(38) | |
| $\chi_{aa}N_a$ | 2.5169 | 2.4744 | -0.0703 | 2.4342(22) | |
| $\chi_{bb}N_a$ | -4.3096 | -4.2442 | 0.2031 | -4.1223(34) | |
| $\chi_{cc}N_a$ | 1.7927 | 1.7698 | -0.1327 | 1.6881(34) | |
| $\mu_a$ [e] | -1.02 | -0.98 | -0.01 | Obs. | |
| $\mu_b$ [e] | -1.17 | -1.15 | -0.05 | Obs. | |
| $\mu_c$ [e] | 0.17 | 0.19 | -0.01 | - | |
| | Cycloserine **II** | | | | |
| | Equilibrium | | $\Delta$vib[b] | Exp. (Species 2) | |
| | rDSD | DZF12[c] | B3 | $B_0$ | $B_e^{semi}$ |
| A | 3664.49 | 3671.29 | -39.70 | 3648.9848(35) | 3688.68 |
| B | 3174.17 | 3180.92 | -23.61 | 3168.6374(18) | 3192.23 |
| C | 1999.02 | 2004.80 | -19.57 | 1993.74394(54) | 2013.33 |
| $\chi_{aa}N_r$ [d] | 4.8387 | 4.7713 | -0.0113 | 4.7662(52) | |
| $\chi_{bb}N_r$ | -1.0336 | -1.0532 | 0.0764 | -0.9912(32) | |
| $\chi_{cc}N_r$ | -3.8051 | -3.7181 | -0.0661 | -3.7750(32) | |
| $\chi_{aa}N_a$ | -0.8411 | -0.8419 | -0.0718 | -0.8781(64) | |
| $\chi_{bb}N_a$ | -1.0725 | -1.0572 | 0.1094 | -1.00898(32) | |
| $\chi_{cc}N_a$ | 1.9136 | 1.8990 | -0.0376 | 1.8871(32) | |
| $\mu_a$ [e] | 1.75 | 1.71 | 0.02 | Obs. | |
| $\mu_b$ [e] | 0.11 | 0.13 | 0.03 | - | |
| $\mu_c$ [e] | -0.37 | -0.35 | 0.01 | - | |

[a] Rotational constants: A, B, C; nuclear quadrupole coupling constants: $\chi_{ii}$; electric dipole moment components: $\mu_i$; where: $i$=$a$, $b$, $c$. [b] Vibrational corrections to spectroscopic parameters (at T = 0 K). [c] Nuclear quadrupole coupling constants computed at the CCSD(T)/jun-cc-pVTZ level. [d] $N_r$ denotes the nitrogen atom in the ring, $N_a$ the amino nitrogen. [e] Values in debye.

for the **II** structure. A summary of these first assignments is provided in the SI (Table S5).

While rotational constants are strongly related to the mass distribution, the nuclear quadrupole hyperfine pattern critically depends on the electronic environment, position and orientation of the $^{14}$N nuclei. Therefore, the nitrogen quadrupole coupling constants ($\chi_{ii}$, with $i = a,b,c$[33]) provide a different and independent source of structural information. Indeed, they have been used as fingerprints in the conformational analysis of amino acids[61,62] as well as for the identification of nucleobase tautomers.[63] The predicted values of the $^{14}N_r$ and $^{14}N_a$ quadrupole coupling constants (see Table 1) are different for **I** and **II** because of the their quite different environments, thus providing a significant aid for determining the position of the ring nitrogen (and, consequently, the ring puckering) as well as the orientation of the $NH_2$ group. Indeed, as it can be seen in Table S2, these constants dramatically change (even in sign) upon variation of the latter parameters.

Being necessary to resolve and interpret the complex hyperfine structure originating from nuclear quadrupole coupling, as mentioned in the experimental details section, the higher resolution (sub-Doppler) of a narrow-band LA-MB-FTMW spectrometer was exploited. As shown in Figures 2b and 4, this instrument is able to fully resolve the hyperfine structure due to the $^{14}$N nuclei, with the $2_{12}$-$1_{01}$ and $2_{12}$-$1_{11}$ transitions being the first analyzed. This choice was based on QC predictions that suggested for these transitions the most spread hyperfine structure. Furthermore, the support of QC calculations made it possible to interpret the complicated quadrupole coupling patterns shown in Figure 4 and led to the assignment of a large number of hyperfine components. Overall, a total of 64 and 47 hyperfine components for **I** and **II**, respectively, was assigned (see Tables S6 and S7 of the SI). They were fitted[64] using the Watson's rigid-rotor Hamiltonian[59] (A reduction, $I^r$ representation ), supplemented by a term[33] to account for the nuclear quadrupole interactions, with the coupling scheme I+J=F, with $I=I_1+I_2$, being used. The resulting nuclear quadrupole coupling constants of both species are compared with the computational counterparts in Table 1, where a quantitative agreement can be noticed.

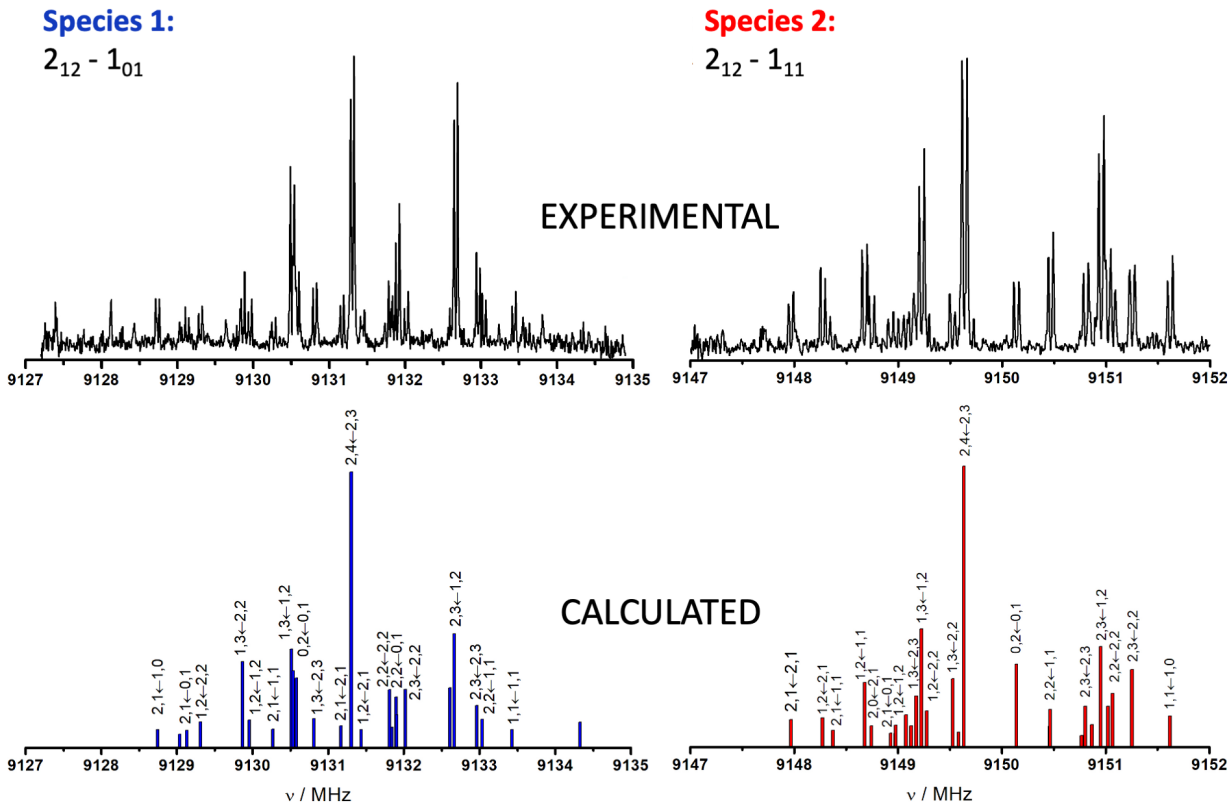


Figure 4: Hyperfine structures of the $2_{12}$-$1_{01}$ and $2_{12}$-$1_{11}$ transitions of Species 1 (left) and Species 2 (right): comparison between experiment and theory.

As mentioned in the Introduction, cycloserine contains the isoxazolidine scaffold. Our study provides the unique opportunity to accurately determine the structural parameters of this five-membered ring, and investigate how these are affected by ring-substituents. It is the presence of a single N-O bond in a saturated ring that makes the isoxazolidine moiety of great relevance in organic and medicinal chemistry.[14] Table 2 reports the main geometrical parameters of the five-membered ring for **I** and **II** evaluated at the rDSD and DZF12 levels, which are compared with those of isoxazolidine computed at the same levels of theory. Furthermore, to benchmark the results obtained, the smallest molecule containing a single N-O bond, hydroxilamine (Figure 1**a**), has been investigated. For the latter, in addition to structural determinations at the rDSD and DZF12 levels, an accurate structural evaluation has been obtained by exploiting the semi-experimental equilibrium structure approach, which

is detailed in the SI. Briefly, the experimental ground-state rotational constants of different isotopologues of hydroxilamine[65] have been corrected for vibrational effects at the B3 level, thus leading to the semi-experimental equilibrium rotational constants. From a least-squares fit of the latter (actually of the corresponding moments of inertia, see the SI for details), the so-called semi-experimental equilibrium structure has been determined. This is shown in Figure S6 and compared with rDSD and DZF12 results in Table S3 of the SI, while the determinations for the N-O distance are also reported in Table 2. Noted is that the semi-experimental approach has also been applied to the evaluation of the N-O bond length in **I** and **II**, while keeping the other structural parameters fixed at the DZF12 values.

Focusing on hydroxilamine, from the inspection of Tables 2 and S3, it is apparent that

**Table 2: Structural parameters[a] of cycloserine and related species employing the atom numbering given in Figure 1.**

| | rDSD | DZF12 | Semi-exp[b] |
|---|---|---|---|
| cycloserine **I**[c] | | | |
| N-O | 1.4287 [1.4271] | 1.4300 [1.4287] | 1.4219(4) [1.4230(1)] |
| O-$C_5$ | 1.4346 [1.4399] | 1.4325 [1.4376] | |
| $C_4$-$C_5$ | 1.5235 [1.5193] | 1.5231 [1.5192] | |
| $C_3$-$C_4$ | 1.5340 [1.5345] | 1.5336 [1.5343] | |
| N-$C_3$ | 1.3807 [1.3836] | 1.3840 [1.3872] | |
| $\theta$ | -13.82 [163.49] | -13.23 [164.40] | |
| **q** | 0.371 [0.379] | 0.378 [0.387] | |
| $\omega$ | 41.96 [-42.62] | 43.74 [-44.57] | |
| $\tau$ | 307.32 [301.13] | 307.11 [301.15] | |
| isoxazolidine[d] | | | |
| N-O | 1.4306 | 1.4297 | |
| O-$C_5$ | 1.4327 | 1.4306 | |
| $C_4$-$C_5$ | 1.5363 | 1.5361 | |
| $C_3$-$C_4$ | 1.5453 | 1.5449 | |
| N-$C_3$ | 1.4687 | 1.4685 | |
| $\theta$ | 14.95 | 14.80 | |
| **q** | 0.384 | 0.388 | |
| $\omega$ | -62.99 | -63.46 | |
| hydroxylamine | | | |
| N-O | 1.4420 | 1.4402 | 1.44086(2) |

[a] Distances in Å, angles in degrees. [b]Semi-experimental equilibrium structure. [c] In square brackets, the parameters for cycloserine **II** are reported. [d] A second enantiomer exists with $\theta_2 = \theta + 180°$, $\mathbf{q}_2 = \mathbf{q}$ and $\omega_2 = -\omega$.

there is a very good agreement between the DZF12 and semi-experimental geometrical parameters, the deviations of the former with respect to the latter being within 0.001 Å for distances and 0.1° for angles. It is furthermore noted that, despite its limited computational cost, the rDSD level performs well, the largest deviation being 0.003 Å for bond lengths and 0.1° for angles. Based on the results of hydroxilamine, the accuracy of the DZF12 level of theory is impressive and further confirms what already pointed out in the discussion of rotational and nitrogen quadrupole coupling constants. By comparing the ring distances of **I** and **II**, it is apparent that they are little affected by the different pseudo-rotation phases, with the N-O bond length changing by less than 0.001 Å. This is also confirmed by the semi-experimental equilibrium distance, which is shorter than the DZF12 counterpart by about 0.008 Å in **I** and 0.006 Å in **II**. However, since all the other parameters have been kept fixed to the DZF12 values in the semi-experimental approach, the overall consequence is that their (even small) errors affect the N-O determination. Therefore, the statistical errors reported in Table 2 cannot be trusted, a more reliable error estimate being 0.003-0.005 Å. Moving to isoxazolidine, the **I** and **II** structures of cycloserine become enantiomers and, at the DZF12 level, the axial placement of the NH hydrogen becomes significantly more stable than the equatorial one (by 478.2 $cm^{-1}$), the N-O distance is unchanged with respect to **I** and the O-$C_5$ bond differs by only ∼0.002 Å. Concerning the other bond lengths, $C_3$-$C_4$ and $C_4$-$C_5$ elongate by a little bit more than 0.01 Å, while $C_3$-N shows the largest difference, nearly 0.09 Å. The latter variation is surely related to the different hybridization ($sp^2$ vs. $sp^3$) of $C_3$ in cycloserine and isoxazolidine. This also explains the variation of about 30° of $\theta$, whereas **q** remains essentially unchanged. Finally, the N-O distance shortens only by about 0.01 Å when moving from hydroxilamine to the five-membered ring, thus suggesting that its nature remains unchanged. Once again, analogous trends are predicted by the much cheaper rDSD computational model with a marginally lower accuracy for all the geometrical parameters.

# Conclusion

In conclusion, state-of the-art quantum-chemical computations show that the small but highly flexible cycloserine has eleven energy minima, which are structurally related to the isoxazolidine ring puckering, the NH inversion, and the rotation of the $NH_2$ group. Characterization of the saddle points ruling the interconversion among the different energy minima suggests the relaxation of all structures to **I** and **II**, which should therefore be the only ones observable by microwave spectroscopy. This prediction has been fully confirmed by experiment, which led to spectroscopic parameters in remarkable agreement with the computed ones. The investigation has also been extended to structural determinations and allowed us to provide the first quantitative description of the structure of the isoxazolidine ring, an important scaffold in medicinal chemistry.

Finally, together with the intrinsic interest of cycloserine, the present study shows that integrated computational-experimental studies allow an unbiased analysis and interpretation of flat and intricate potential energy surfaces for flexible molecules in terms of structural and spectroscopic parameters.

# Acknowledgement

This work has been supported by the Ministerio de Ciencia e Innovación (CTQ2016-76393-P and PID2019-111396GB-I00), Junta de Castilla y León (Grants VA077U16 and VA244P20) and the European Research Council ERC-2013-SyG, n. 610256 NANOCOSMOS, MIUR 'PRIN 2017' (Grant Number 2017A4XRCA), and by the Italian Space Agency (ASI; 'Life in Space' project, N. 2019-3-U.0). E.R.A. acknowledges the Fundación Biofísica Bizkaia for a postdoctoral grant.

## Supporting Information Available

Conformational analysis details; computational methods details; geometric parameters and relative energies of each conformation; Cartesian coordinates in xyz format of the two detected conformers; isoxazolidine and hydroxilamine computational results; Measured transition frequencies and residuals (in MHz) for the hyperfine components of the rotational transitions of the cycloserine species measured by the LA-CP-FTMW and the LA-MB-FTMW spectrometers.

# References


(1) Polc, P.; Pieri, L.; Bonetti, E.; Scherschlicht, R.; Moehler, H.; Kettler, R.; Burkard, W.; Haefely, W. l-Cycloserine: Behavioural and biochemical effects after single and repeated administration to mice, rats and cats. *Neuropharmacology* **1986**, *25*, 411–418.

(2) Kuehl, F. A.; Wolf, F. J.; Trenner, N. R.; Peck, R. L.; Buhs, R. P.; Howe, E.; Putter, I.; Hunnewell, B. D.; Ormond, R.; Downing, G. et al. D-4-amino-3-isoxazolidone, a new antibiotic. *J. Am. Chem. Soc.* **1955**, *77*, 2344–2345.

(3) Stammer, C. H.; Wilson, A. N.; Holly, F. W.; Folkers, K. SYnthesis of D-4-amino-3-isoxazolidone. *J. Am. Chem. Soc.* **1955**, *77*, 2346–2347.

(4) Dall'Olio, R.; Gandolfi, O.; Gaggi, R. D-Cycloserine, a positive modulator of NMDA receptors, inhibits serotonergic function. *Behav. Pharmacol.* **2000**, *11*, 631–637.

(5) Otto, M. W.; Olin, D. F.; Simon, M. N.; Pearlson, G. D.; Basden, S. A. E., S.and Meunier; Hoffmann, S. G.; Eisenmerger, K.; Krystal, J. H.; Pollack, M. H. Efficacy of D-Cycloserine for Enhancing Response to Cognitive-Behavior Therapy for Panic Disorder. *Biol. Psychiatry* **2010**, *67*, 365–370.

(6) Chasson, G. S.; Buhlmann, U.; Tolin, D. F.; Rao, S. R.; Reese, H.; Rowley, T.; Welsh, S., K.S.and Wilhelm Need for speed: Evaluating slopes of OCD recovery in behavior therapy enhanced with d-cycloserine. *Behav. Res. Ther.* **2010**, *48*, 675–679.

(7) Kaushal, G.; Ramirez, R.; Alambo, D.; Taupradist, W.; Choksi, K.; Sirbu, C. Initial characterization of D-cycloserine for future formulation development for anxiety disorders. *Drug Discovery Ther.* **2011**, *5*, 253–260.

(8) Hidy, P. H.; Hodge, E. B.; Young, V. V.; Harned, R. L.; Brewer, G. A.; Phillips, W. F.; Runge, W. F.; Stavely, H. E.; Pohland, A.; Boaz, H. et al. Structure and reactions of cycloserine. *J. Am. Chem. Soc.* **1955**, *77*, 2345–2346.

(9) Iakhontova, L.; Bruns, B.; Kartseva, V.; Kobzieva, S.; Perevozskaia, N. [Physico-chemical and sorption properties of d-cycloserine]. *Antibiotiki* **1969**, *14*, 205—210.

(10) Yosa, J.; Blanco, M.; Acevedo, O.; Lareo, L. Molecular orbital differentiation of agonist and antagonist activity in the GlycineB-iGluR-NMDA receptor. *Eur. J. Med. Chem.* **2009**, *44*, 2960 – 2966.

(11) Fraschetti, C.; Filippi, A.; Borocci, S.; Steinmetz, V.; Speranza, M. Isomerism of Cycloserine and Its Protonated Form. *ChemPlusChem* **2014**, *79*, 584–591.

(12) Filippi, A.; Fraschetti, C.; Grandinetti, F.; Speranza, M.; Ponzi, A.; Decleva, P.; Stranges, S. Electronic structure and conformational flexibility of d-cycloserine. *Phys. Chem. Chem. Phys.* **2015**, *17*, 25845–25853.

(13) Ahmed, M.; Wang, F.; Acres, R. G.; Prince, K. C. Structures of Cycloserine and 2-Oxazolidinone Probed by X-ray Photoelectron Spectroscopy: Theory and Experiment. *J. Phys. Chem. A* **2014**, *118*, 3645–3654.

(14) Berthet, M.; Cheviet, T.; Dujardin, G.; Parrot, I.; Martinez, J. Isoxazolidine: A Privileged Scaffold for Organic and Medicinal Chemistry. *Chem. Rev.* **2016**, *116*, 15235–15283.

(15) Puzzarini, C.; Stanton, J. F.; Gauss, J. Quantum-chemical calculation of spectroscopic parameters for rotational spectroscopy. *Int. Rev. Phys. Chem.* **2010**, *29*, 273–367.

(16) Puzzarini, C.; Barone, V. Diving for Accurate Structures in the Ocean of Molecular Systems with the Help of Spectroscopy and Quantum Chemistry. *Acc. Chem. Res.* **2018**, *51*, 548–556.

(17) Alonso, E. R.; León, I.; Alonso, J. L. *Intra- and Intermolecular Interactions Between Non-covalently Bonded Species*; Elsevier, 2021; pp 93–141.

(18) Alonso, J. L.; López, J. C. In *Gas-Phase IR Spectroscopy and Structure of Biological Molecules*; Rijs, A. M., Oomens, J., Eds.; Springer International Publishing: Cham, 2015; pp 335–401.

(19) Puzzarini, C.; Biczysko, M.; Barone, V.; Largo, L.; Peña, I.; Cabezas, C.; Alonso, J. L. Accurate Characterization of the Peptide Linkage in the Gas Phase: A Joint Quantum-Chemical and Rotational Spectroscopy Study of the Glycine Dipeptide Analogue. *J. Phys. Chem. Lett* **2014**, *5*, 534–540.

(20) León, I.; Alonso, E. R.; Mata, S.; Cabezas, C.; Alonso, J. L. Unveiling the Neutral Forms of Glutamine. *Angew. Chem. Int. Ed. Engl.* **2019**, *58*, 16002–16007.

(21) León, I.; Alonso, E. R.; Cabezas, C.; Mata, S.; Alonso, J. L. Unveiling the $n \rightarrow \pi^*$ interactions in dipeptides. *Commun. Chem.* **2019**, *2*, 3.

(22) Simão, A.; Cabezas, C.; León, I.; Alonso, E. R.; Mata, S.; Alonso, J. L. Elucidating the multiple structures of pipecolic acid by rotational spectroscopy. *Phys. Chem. Chem. Phys.* **2019**, *21*, 4155–4161.

(23) Puzzarini, C.; Bloino, J.; Tasinato, N.; Barone, V. Accuracy and Interpretability: The Devil and the Holy Grail. New Routes across Old Boundaries in Computational Spectroscopy. *Chem. Rev.* **2019**, *119*, 8131–8191.

(24) Li, W.; Spada, L.; Tasinato, N.; Rampino, S.; Evangelisti, L.; Gualandi, A.; Cozzi, P. G.; Melandri, S.; Barone, V.; Puzzarini, C. Theory Meets Experiment for Noncovalent Complexes: The Puzzling Case of Pnicogen Interactions. *Angew. Chem. Int. Ed.* **2018**, *57*, 13853–13857.

(25) Obenchain, D. A.; Spada, L.; Alessandrini, S.; Rampino, S.; Herbers, S.; Tasinato, N.; Mendolicchio, M.; Kraus, P.; Gauss, J.; Puzzarini, C. et al. Unveiling the Sulfur–Sulfur Bridge: Accurate Structural and Energetic Characterization of a Homochalcogen Intermolecular Bond. *Angew. Chem. Int. Ed.* **2018**, *57*, 15822–15826.

(26) Wang, J.; Spada, L.; Chen, J.; Gao, S.; Alessandrini, S.; Feng, G.; Puzzarini, C.; Gou, Q.; Grabow, J.-U.; Barone, V. The Unexplored World of Cycloalkene–Water Complexes: Primary and Assisting Interactions Unraveled by Experimental and Computational Spectroscopy. *Angew. Chem. Int. Ed.* **2019**, *58*, 13935–13941.

(27) Cabezas, C.; Varela, M.; Alonso, J. L. The Structure of the Elusive Simplest Dipeptide Gly-Gly. *Angew. Chem. Int. Ed.* **2017**, *56*, 6420–6425.

(28) León, I.; Peña, I.; Cabezas, C.; Alonso, E. R.; Alonso, J. L. The last link of the x-aminobutyric acid series: the five conformers of $\hat{\mathrm{I}}^{\mathbf{2}}$-aminobutyric acid. *Phys. Chem. Chem. Phys.* **2018**, *20*, 15574–15580.

(29) León, I.; Alonso, E. R.; Mata, S.; Alonso, J. L. A rotational study of the AlaAla dipeptide. *Phys. Chem. Chem. Phys.* **2020**, *22*, 13867–13871.

(30) Ruoff, R. S.; Klots, T. D.; Emilsson, T.; Gutowsky, H. S. Relaxation of conformers and isomers in seeded supersonic jets of inert gases. *J. Chem. Phys.* **1990**, *93*, 3142–3150.

(31) Godfrey, P. D.; Brown, R. D.; Rodgers, F. M. The missing conformers of glycine and alanine: relaxation in seeded supersonic jets. *J. Mol. Struct.* **1996**, *376*, 65 – 81.

(32) Alonso, J. L.; Peña, I.; López, J. C.; Alonso, E. R.; Vaquero, V. The Shape of the Simplest Non-proteinogenic Amino Acid $\alpha$-Aminoisobutyric Acid (Aib). *Chem. Eur. J.* **2019**, *25*, 2288–2294.

(33) Gordy, W.; Cook, R. L. *Microwave molecular spectra*; Wiley, 1984.

(34) Puzzarini, C. Rotational spectroscopy meets theory. *Phys. Chem. Chem. Phys.* **2013**, *15*, 6595–6607.

(35) Barone, V.; Ceselin, G.; Fusè, M.; Tasinato, N. Accuracy Meets Interpretability for Computational Spectroscopy by Means of Hybrid and Double-Hybrid Functionals. *Front. Chem.* **2020**, *8*, 859.

(36) Xie, F.; Fusè, M.; Hazrah, A. S.; Jaeger, W.; Barone, V.; Xu, Y. Discovering the elusive global minimum in a ternary chiral cluster: rotational spectra of propylene oxide trimer. *Angew. Chem. Int. Ed.* **2020**, *59*, 22427–22430.

(37) Santra, G.; Sylvetsky, N.; Martin, J. M. L. Minimally Empirical Double-Hybrid Functionals Trained against the GMTKN55 Database: revDSD-PBEP86-D4, revDOD-PBE-D4, and DOD-SCAN-D4. *J. Phys. Chem. A* **2019**, *123*, 5129–5143.

(38) Dunning, T. H. Gaussian Basis Sets for Use in Correlated Molecular Calculations. I. The Atoms Boron Through Neon and Hydrogen. *J. Chem. Phys.* **1989**, *90*, 1007–1023.

(39) Papajak, E.; Zheng, J.; Xu, X.; Leverentz, H. R.; Truhlar, D. G. Perspectives on Basis Sets Beautiful: Seasonal Plantings of Diffuse Basis Functions. *J. Chem. Theory Comput.* **2011**, *7*, 3027–3034.

(40) Grimme, S.; Ehrlich, S.; Goerigk, L. Effect of the Damping Function in Dispersion Corrected Density Functional Theory. *J. Comput. Chem.* **2011**, *32*, 1456–1465.

(41) Knizia, G.; Adler, T. B.; Werner, H.-J. Simplified CCSD(T)-F12 methods: Theory and benchmarks. *J. Chem. Phys.* **2009**, *130*, 054104.

(42) Lupi, J.; Puzzarini, C.; Cavallotti, C.; Barone, V. State-of-the-Art Quantum Chemistry Meets Variable Reaction Coordinate Transition State Theory to Solve the Puzzling Case of the H2S + Cl System. *J. Chem. Theory Comput.* **2020**, *16*, 5090–5104.

(43) Salta, Z.; Segovia, E., M.; Katz, A.; Tasinato, N.; Barone, V.; Ventura, N., O. Isomerization and Fragmentation Reactions on the [C2SH4] Potential Energy Surface: The Metastable Thione S-Methylide Isomer. *J. Org. Chem.* **2020**, *86*, 2941–2956.

(44) Peterson, K. A.; Adler, T. B.; Werner, H.-J. Systematically convergent basis sets for explicitly correlated wavefunctions: The atoms H, He, B–Ne, and Al–Ar. *J. Chem. Phys.* **2008**, *128*, 084102.

(45) Raghavachari, K.; Trucks, G. W.; Pople, J. A.; Head-Gordon, M. A fifth-order perturbation comparison of electron correlation theories. *Chem. Phys. Lett.* **1989**, *157*, 479 – 483.

(46) Spackman, R., Peter; Jayatilaka, D.; Karton, A. Basis set convergence of CCSD(T) equilibrium geometries using a large and diverse set of molecular structures. *J. Chem. Phys.* **2016**, *145*, 104101.

(47) Becke, A. D. Density-functional exchange-energy approximation with correct asymptotic behavior. *Phys. Rev. A* **1988**, *38*, 3098–3100.

(48) Bloino, J.; Biczysko, M.; Barone, V. General perturbative approach for spectroscopy, thermodynamics, and kinetics: Methodological background and benchmark studies. *J. Chem. Theory Comput.* **2012**, *8*, 1015–1036.

(49) Brown, G. G.; Dian, B. C.; Douglass, K. O.; Geyer, S. M.; Shipman, S. T.; Pate, B. H. A broadband Fourier transform microwave spectrometer based on chirped pulse excitation. *Rev. Sci. Instrum.* **2008**, *79*, 053103.

(50) Mata, S.; Peña, I.; Cabezas, C.; López, J.; Alonso, J. A broadband Fourier-transform microwave spectrometer with laser ablation source: The rotational spectrum of nicotinic acid. *J. Mol. Spectrosc.* **2012**, *280*, 91 – 96, Broadband Rotational Spectroscopy.

(51) Peña, I.; Mata, S.; Martín, A.; Cabezas, C.; Daly, A. M.; Alonso, J. L. Conformations of d-xylose: the pivotal role of the intramolecular hydrogen-bonding. *Phys. Chem. Chem. Phys.* **2013**, *15*, 18243–18248.

(52) Bermúdez, C.; Mata, S.; Cabezas, C.; Alonso, J. L. Tautomerism in Neutral Histidine. *Angew. Chem. Int. Ed.* **2014**, *53*, 11015–11018.

(53) León, I.; Alonso, E. R.; Mata, S.; Cabezas, C.; Rodríguez, M. A.; Grabow, J.-U.; Alonso, J. L. The role of amino acid side chains in stabilizing dipeptides: the laser

ablation Fourier transform microwave spectrum of Ac-Val-NH2. *Phys. Chem. Chem. Phys.* **2017**, *19*, 24985–24990.

(54) Andresen, U.; Dreizler, H.; Grabow, J.; Stahl, W. An automatic molecular beam microwave Fourier transform spectrometer. *Rev. Sci. Instrum.* **1990**, *61*, 3694–3699.

(55) Grabow, J.; Stahl, W.; Dreizler, H. A multioctave coaxially oriented beam-resonator arrangement Fourier-transform microwave spectrometer. *Rev. Sci. Instrum.* **1996**, *67*, 4072–4084.

(56) Cremer, D. T.; Pople, J. A. General definition of ring puckering coordinates. *J. Am. Chem. Soc.* **1975**, *97*, 1354–1358.

(57) Paoloni, L.; Rampino, S.; Barone, V. Potential-Energy Surfaces for Ring-Puckering Motions of Flexible Cyclic Molecules through Cremer–Pople Coordinates: Computation, Analysis, and Fitting. *J. Chem. Theory Comput.* **2019**, *15*, 4280–4294.

(58) Cahn, R. S.; Ingold, C.; Prelog, V. Specification of Molecular Chirality. *Angew. Chem. Int. Ed. Engl.* **1966**, *5*, 385–415.

(59) Watson, J. K. *Vibrational spectra and structure*; Elsevier: Amsterdam, 1977.

(60) Kolesniková, L.; León, I.; Alonso, E. R.; Mata, S.; Alonso, J. L. Laser Ablation Assists Cyclization Reactions of Hydantoic Acid: A Proof for the Near-Attack Conformation Theory? J. *J. Phys. Chem. Lett.* **2019**, *10*, 1325–1330.

(61) Cabezas, C.; Varela, M.; Peña, I.; Mata, S.; López, J. C.; Alonso, J. L. The conformational locking of asparagine. *Chem. Commun.* **2012**, *48*, 5934–5936.

(62) Peña, I.; Sanz, M. E.; López, J. C.; Alonso, J. L. Preferred Conformers of Proteinogenic Glutamic Acid. *J. Am. Chem. Soc.* **2012**, *134*, 2305–2312.

(63) Alonso, J. L.; Vaquero, V.; Peña, I.; López, J. C.; Mata, S.; Caminati, W. All Five Forms of Cytosine Revealed in the Gas Phase. *Angew. Chem. Int. Ed.* **2013**, *52*, 2331–2334.

(64) Pickett, H. M. The fitting and prediction of vibration-rotation spectra with spin interactions. *J. Mol. Spectrosc.* **1991**, *148*, 371 – 377.

(65) Tsunekawa, S. Microwave Spectrum of Hydroxylamine. *J. Phys. Soc. Jpn.* **1972**, *33*, 167–174.

# Graphical TOC Entry